Test–Retest Reproducibility of Binding Parameters in Humans with ^{11}C-LY2795050, an Antagonist PET Radiotracer for the κ Opioid Receptor

Mika Naganawa[1], Ming-Qiang Zheng[1], Shannan Henry[1], Nabeel Nabulsi[1], Shu-Fei Lin[1], Jim Ropchan[1], David Labaree[1], Soheila Najafzadeh[1], Michael Kapinos[1], Johannes Tauscher[2], Alexander Neumeister[3], Richard E. Carson[1], and Yiyun Huang[1]

[1]PET Center, Department of Diagnostic Radiology, Yale University School of Medicine, New Haven, Connecticut; [2]Eli Lilly and Co., Indianapolis, Indiana; and [3]Department of Psychiatry and Radiology, New York University School of Medicine, New York, New York

^{11}C-LY2795050 is a new antagonist PET radioligand for the κ opioid receptor (KOR). In this study, we assessed the reproducibility of the binding parameters of ^{11}C-LY2795050 in healthy human subjects. **Methods:** Sixteen healthy subjects (11 men and 5 women) underwent 2 separate 90-min PET scans with arterial input function and plasma free fraction (f_P) measurements. The 2-tissue-compartment model and multilinear analysis-1 were applied to calculate 5 outcome measures in 14 brain regions: distribution volume (V_T), V_T normalized by f_P (V_T/f_P), and 3 binding potentials (nondisplaceable binding potential, binding potential relative to total plasma concentration, and binding potential relative to free plasma concentration: BP_{ND}, BP_P, BP_F, respectively). Since KOR is distributed ubiquitously throughout the brain, there are no suitable reference regions. We used a fixed fraction of individual cerebellar V_T value ($V_{T,CER}$) as the nondisplaceable V_T (V_{ND}) ($V_{ND} = V_{T,CER}/1.17$). The relative and absolute test–retest variability and intraclass correlation coefficient were evaluated for the outcome measures of ^{11}C-LY2795050. **Results:** The test–retest variability of ^{11}C-LY2795050 for V_T was no more than 10% in any region and was 12% in the amygdala. For binding potential (BP_{ND} and BP_P), the test–retest variability was good in regions of moderate and high KOR density ($BP_{ND} > 0.4$) and poor in regions of low density. Correction by f_P (V_T/f_P or BP_F) did not improve the test–retest performance. **Conclusion:** Our results suggest that quantification of ^{11}C-LY2795050 imaging is reproducible and reliable in regions with moderate and high KOR density. Therefore, we conclude that this first antagonist radiotracer is highly useful for PET studies of KOR.

Key Words: kappa opioid receptor; positron emission tomography; test–retest reproducibility; brain imaging

J Nucl Med 2015; 56:243–248
DOI: 10.2967/jnumed.114.147975

The κ opioid receptor (KOR) is 1 of at least 3 subtypes of opioid receptor. KOR is known to be involved in various disorders, including anxiety (*1*), substance abuse (*2*), major depression (*3,4*), epilepsy (*5*), and Alzheimer disease (*6*). Several lines of work provide support for KOR antagonists as potential therapeutic agents for depression (*7*) and alcohol dependence (*8*).

The PET radioligand ^{11}C-LY2795050 is a recently developed antagonist radiotracer (*9*) that binds selectively to KOR. This new tracer has been examined in both nonhuman primates (*10,11*) and human subjects (*12*). Our previous analysis of human imaging data found that a 150-mg oral dose of naltrexone blocked approximately 90% of KORs across all brain regions, suggesting the absence of a suitable reference region for ^{11}C-LY2795050 in the human brain and that the lowest intersubject variability in 3 versions of binding potential (nondisplaceable binding potential, binding potential relative to total plasma concentration, and binding potential relative to free plasma concentration: BP_{ND}, BP_P, BP_F, respectively) was observed when the nondisplaceable V_T (V_{ND}) was estimated as a fixed fraction of cerebellar V_T ($V_{T,CER}$) ($V_{ND} = V_{T,CER}/1.17$). The uptake pattern of ^{11}C-LY2795050 agreed well with the known KOR distribution, and ^{11}C-LY2795050 was confirmed to be suitable for imaging KOR in vivo. The primary aim of the present study was to assess the test–retest variability (TRV) of ^{11}C-LY2795050 binding parameters derived from kinetic modeling in the human brain.

MATERIALS AND METHODS

Human Subjects

Sixteen healthy subjects (19–42 y old; 11 men and 5 women; body weight, 79 ± 11 kg) were enrolled in a test–retest study. The study was approved by the Yale University Human Investigation Committee and the Yale–New Haven Hospital Radiation Safety Committee and was in accordance with the federal guidelines and regulations of the United States for the protection of human research subjects contained in Title 45 part 46 of the Code of Federal Regulations. All subjects provided written informed consent. As part of the subject evaluation, MR images were acquired on all subjects to eliminate those with anatomic abnormalities and for PET image registration. MR imaging was performed using a 3-dimensional magnetization-prepared rapid gradient-echo pulse sequence with an echo time of 2.78 ms, repetition time of 2,500 ms, inversion time of 1,100 ms, and flip angle of 7 on a 3-T whole-body scanner (Trio; Siemens Medical Systems) with a circularly polarized head coil. The dimensions and pixel size of the MR images were 256 × 256 × 176 matrix and 0.98 × 0.98 × 1.0 mm^3, respectively.

Radiotracer Synthesis

^{11}C-LY2795050 was synthesized as previously described (*9*). The radiochemical purity of ^{11}C-LY2795050 in the final product solution was more than 98%.

Received Oct. 3, 2014; revision accepted Nov. 20, 2014.
For correspondence or reprints contact: Mika Naganawa, Yale University, 801 Howard Ave., P.O. Box 208048, New Haven, CT 06520-8048.
E-mail: mika.naganawa@yale.edu
Published online Jan. 15, 2015.

Test–Retest Study

Each subject underwent two 90-min PET scans with ^{11}C-LY2795050 on the same day. The time difference between the 2 scans was 4.6 ± 1.1 h. The PET scans were acquired on a High Resolution Research Tomograph (HRRT) (Siemens Medical Solutions), which acquires 207 slices (1.2-mm slice separation) with a reconstructed image resolution of about 3 mm. Before tracer administration, a 6-min transmission scan was conducted for attenuation correction. Each scan was acquired in list mode after intravenous administration of ^{11}C-LY2795050 over 1 min by an automatic pump (Harvard PHD 22/2000; Harvard Apparatus). Dynamic scan data were reconstructed in 27 frames (6 × 0.5 min, 3 × 1 min, 2 × 2 min, and 16 × 5 min) with correction for attenuation, normalization, scatter, randoms, and dead time using the MOLAR algorithm (motion-compensation ordered-subsets expectation maximization list-mode algorithm for resolution-recovery reconstruction) (*13,14*). Motion correction was included in the reconstruction algorithm based on measurements from the Polaris Vicra sensor (NDI Systems) with reflectors mounted on a swim cap worn by the subject. The metabolite-corrected arterial input function and the plasma free fraction (f_P) were measured. The analysis procedures were previously reported (*12*).

Image Registration and Definition of Regions of Interest

Regions of interest were taken from the Automated Anatomic Labeling for SPM2 (*15*) in Montreal Neurologic Institute space (*16*). The template regions of interest were applied to the PET data. Details on the registration between MR and PET images were reported previously (*12*). Using the combined transformations from template-to-PET space, we generated time–activity curves for 14 regions of interest: amygdala, caudate, centrum semiovale, cerebellum, anterior cingulate cortex, posterior cingulate cortex, frontal cortex, globus pallidus, hippocampus, insula, occipital cortex, putamen, temporal cortex, and thalamus.

Quantitative Analysis

In our previous study (*12*), the 2-tissue-compartment (2TC) model and multilinear analysis-1 (MA1) method (*17*) were both deemed appropriate for analysis and quantification of ^{11}C-LY2795050 binding parameters in the human brain. Hence, in this study we applied 2TC and MA1 ($t^* = 30$ min) to the regional time–activity curves using the arterial plasma time–activity curve as input function. Five outcome measures were calculated: V_T, V_T normalized by f_P (V_T/f_P), BP_{ND}, BP_P, and BP_F (*18*). V_{ND} is required for calculation of binding potential. In our previous analysis with a naltrexone-blocking study in humans, the lowest intersubject variability was observed when V_{ND} was estimated as $V_{T,CER}$. We thus calculated V_{ND} from individual $V_{T,CER}$ to estimate binding potential. All modeling was performed with in-house programs written in IDL 8.0 (ITT Visual Information Solutions). For parameter estimation, data points were weighted on the basis of noise equivalent counts in each frame. Percentage SE was estimated from the theoretic parameter covariance matrix.

Statistical Analyses

The reproducibility of the outcome measures was assessed by computation of relative TRV, absolute TRV (aTRV), and intraclass correlation coefficient (ICC). TRV was calculated as follows:

$$\text{TRV} = \frac{\text{test value} - \text{retest value}}{(\text{test value} + \text{retest value})/2}.$$

Mean TRV is an index of trends in the parameter of interest between the 2 scans, and the SD of TRV is an index of the variability of the percentage difference between the 2 measurements. aTRV combines these 2 effects into a single value. To evaluate within-subject variability relative to between-subject variability, ICC was computed using the following equation:

$$\text{ICC} = \frac{\text{BSMSS} - \text{WSMSS}}{\text{BSMSS} + \text{WSMSS}},$$

where BSMSS indicates the between-subject mean sum of squares and WSMSS indicates the within-subject mean sum of squares.

RESULTS

Injection and Scan Parameters

Injection and scan parameters are listed in Table 1. The injected dose and injected mass did not significantly differ between the test and retest scans ($P > 0.05$, paired t test).

Plasma Analysis

Figure 1 displays the total plasma curves, parent fractions, and metabolite-corrected plasma curves for the test and retest scans. There were no significant differences in the parent fractions between the test and retest scans (Fig. 1B). The parent fraction was 42% ± 9% and 19% ± 6% at 30 and 90 min after injection, respectively ($n = 32$). The f_P of ^{11}C-LY2795050 was 0.0094 ± 0.0014 ($n = 32$). The TRV of f_P was 5% ± 12%, with no significant change between the test and retest scans ($P = 0.11$, paired t test).

Uptake Images

Figure 2 shows template MR images and summed PET images averaged across all subjects and scans. A similar uptake pattern for ^{11}C-LY2795050 was observed in the test and retest scans. High uptake was seen in the amygdala, anterior cingulate cortex, insula, and globus pallidus.

TRV and Reproducibility of Binding Parameters

Regional time–activity curves for representative brain regions under test and retest conditions are shown in Figures 3A and 3B, respectively. The 2TC and MA1 ($t^* = 30$ min) models provided good fits to the regional time–activity curves. MA1 provided reliable V_T estimates, with the relative SE (SE/estimated parameter) being less than 10% in most regions and scans, except for the amygdala in 2 scans (10% and 13%). The 2TC V_T estimates were somewhat less stable, with relative SE being more than 10% or k_4 less than 0.001 min^{-1} in 2.5% of the fits (amygdala [$n = 4$], insula [$n = 1$], globus pallidus [$n = 1$], putamen [$n = 1$], caudate [$n = 3$], and centrum semiovale [$n = 1$]). Excluding these unreliable V_T estimates, V_T values from MA1 and 2TC were nearly identical ($V_{T,MA1} = 1.00\ V_{T,2TC} - 0.02$, $R^2 = 0.99$). The MA1 V_T estimates were used for assessing TRV.

TABLE 1
Subject Information and PET Scan Parameters

Parameter	Test ($n = 16$)	Retest ($n = 16$)
Age (y)	28 ± 7	28 ± 7
Body weight (kg)	78.6 ± 11.4	78.6 ± 11.4
Injected dose (MBq)	390 ± 135	461 ± 178
Specific activity (MBq/nmol)	18.0 ± 6.4	21.8 ± 9.6
Injected mass (μg)	9.1 ± 1.2	9.1 ± 1.3

Data are mean ± SD.

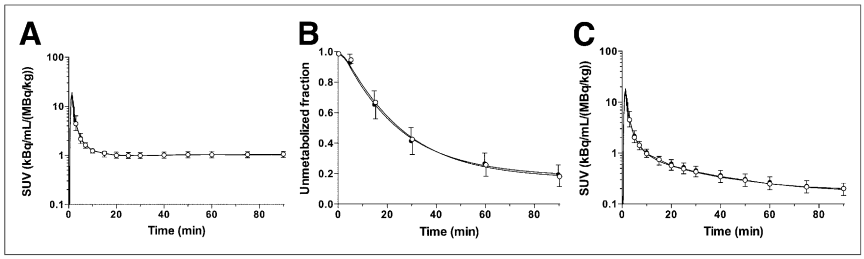

FIGURE 1. Mean ± SD of total plasma activity (A), parent fraction in plasma (B), and metabolite-corrected plasma activity (C) over time after injection of ^{11}C-LY2795050 in test (closed circles, $n = 16$) and retest (open circles, $n = 16$) scans. A and C are displayed in SUV units (concentration/[injected dose/body weight]).

Table 2 shows the outcome measures of interest estimated with MA1 under test and retest conditions. Intersubject variability was 9%–16% for V_T, 16%–21% for V_T/f_P, 14%–46% for BP_{ND}, 8%–41% for BP_P, and 15%–46% for BP_F. Given the relatively small magnitude of BP_{ND} (0.33–1.5) and BP_P (0.52–2.42), higher intersubject variability is to be expected. For the higher-binding regions (e.g., $BP_{ND} > 0.5$), the variability in BP_{ND} and BP_P values was less than 30% and less than or equal to 20%, respectively.

Tables 3 and 4 list the test–retest statistics for V_T and binding potential, respectively. For the V_T estimates, the global mean of TRV and aTRV across all regions was 1% and 7%, respectively. ICC values for the V_T estimates were generally good (>0.6) except for the amygdala (0.41), thalamus (0.54), and centrum semiovale (0.57). The use of f_P to normalize V_T led to poorer reproducibility, with global means of TRV and aTRV at −4% and 14%, respectively. In the regions with moderate to high KOR density ($BP_{ND} > 0.4$), with the exception of the amygdala and hippocampus the TRV had a mean close to zero (no trend between test and retest scans) and an SD of 3%, and the aTRV of the BP_{ND} estimates was lower than 10%. ICC values for the BP_{ND} estimates were greater than 0.8 in all regions except the amygdala (0.56). The global mean of aTRV for BP_F (21%) was significantly higher than that for BP_{ND} (13%) or BP_P (15%).

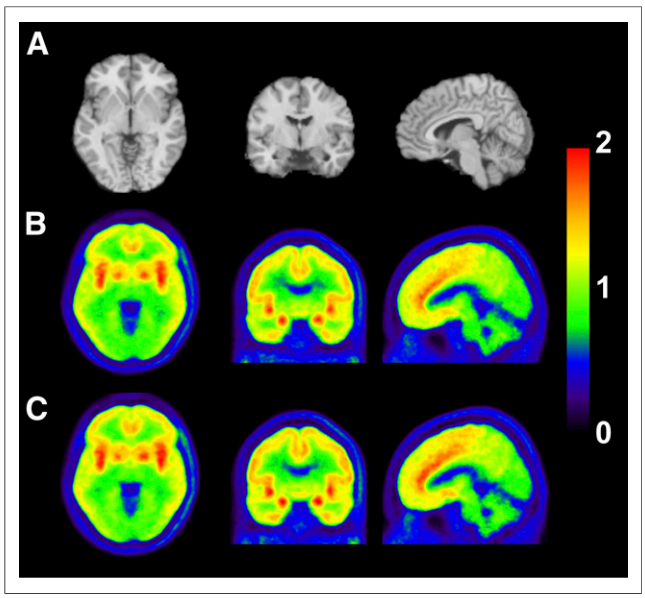

FIGURE 2. MR images and coregistered PET images summed from 30 to 90 min after injection of ^{11}C-LY2795050: MR images (A), test scan (B), and retest scan (C). PET images are displayed in SUV units. SUV images were averaged across all subjects.

DISCUSSION

In this paper, we have presented the TRV and reproducibility of regional binding parameters derived from the KOR antagonist tracer ^{11}C-LY2795050 in the human brain.

In accordance with our previous analysis, the 2TC and MA1 models showed similarly good fits to regional time–activity curves and provided almost identical V_T values. However, V_T estimates with the 2TC model were unstable in some regions. Hence, the MA1 estimates were used for test–retest reproducibility assessment.

The small variability in the injected mass of ^{11}C-LY2795050 was due to the mass limit of 10 μg, which was reached in most scans because of the narrow range of tracer specific activity (Table 1). Receptor occupancy by the carrier mass was calculated from the equation $100 \times F/(F + K_D)$, where F is the mean value (from 60 to 90 min after injection) of the protein-unbound and metabolite-corrected plasma concentration. Using the in vitro (0.72 nmol/L (*9*)) and in vivo (0.028 nmol/L (*12*)) K_D values, we calculated the occupancy by carrier mass in all scans as being less than 0.2% and less than 3%, respectively. In our previous study on rhesus monkeys (*11*), the LY2795050 effective dose for 50% at KOR was estimated as 15.6 μg/kg. With this effective dose, the occupancy by LY2795050 was less than 1.5% in all scans. In either way, the injected tracer occupied less than 5% of the targeted receptor and fulfilled the tracer dose criterion.

f_P was used to calculate normalized V_T (V_T/f_P) and BP_F. If f_P is measured accurately and V_T varies linearly with f_P, the use of f_P for normalization will reduce the TRV or aTRV. However, f_P was too low (<1%) to be measured accurately for this tracer. Moreover, in comparing V_T and binding potential with or without correction by f_P (V_T and V_T/f_P, and BP_P and BP_F), we found that the absolute TRV was higher and ICC lower for the estimates with f_P correction than for the estimates without f_P correction in all regions, because f_P is higher in the test scan than the retest scan. Among the 3 binding potentials, BP_F showed the highest aTRV, which was twice that for BP_{ND}. Normalization of V_T by f_P or binding potential calculated with f_P led to worse test–retest reproducibility and reliability, possibly because of small errors in f_P measurements.

The test–retest performance of ^{11}C-LY2795050 in V_T estimates was excellent across all regions, with mean TRV being close to 0% and aTRV being less than 10%, except for the amygdala and centrum semiovale (aTRV of 12% and 10%, respectively) (Table 3). Similarly, in regions with moderate and high KOR densities, the TRV of BP_{ND} and BP_P estimates was also good. However, in regions with low KOR density (posterior cingulate cortex, thalamus, centrum semiovale), not surprisingly, the variability of BP_{ND} and BP_P was higher than that of V_T. On the basis of these TRV values, the use of binding potential would likely be limited to regions with moderate to high KOR density. In this study, we calculated binding potential with a fixed fraction of individual

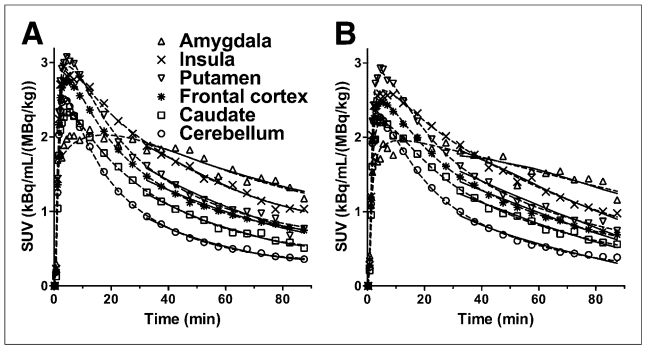

FIGURE 3. Time–activity curves from 1 subject for 6 selected regions after injection of ^{11}C-LY2795050 under test (A) and retest (B) conditions. Fits with MA1 ($t^* = 30$ min) and 2TC models are displayed as solid and dotted lines, respectively.

cerebellar V_T as V_{ND}. An important assumption here is that the fraction does not change between the test and retest scans. Obviously, the use of a fixed fraction of cerebellar V_T as V_{ND} will also need validation in different patient populations by blocking experiments and in subjects under drug challenge conditions. The use of V_T instead of binding potential is most appropriate, and preferred, if this assumption of a fixed fraction of cerebellar V_T as V_{ND} is no longer valid, depending on disease or experimental conditions.

The aTRV in the highest-binding region, amygdala, was more than 10% in all outcome measures although it was lower in other high-binding regions. The likely reason is that its small size led to a noisy time–activity curve.

The development of selective KOR imaging agents has been pursued for a long time (*19*). Although several radiotracers have been developed over the years, thus far only the KOR agonist ^{11}C-GR103545 has been investigated extensively in vivo in nonhuman primates (*20,21*) and humans (*22*) and found to be a suitable radiotracer for KOR imaging and quantification. As part of a comprehensive evaluation in humans, the test–retest performance of ^{11}C-GR103545 was assessed using methods similar to those described above for ^{11}C-LY2795050 (*22*). The mean aTRV of V_T estimate was about 15% for ^{11}C-GR103545, compared with less than 10% for ^{11}C-LY2795050. This difference in the test–retest reproducibility of V_T estimates most likely derives from the kinetic behavior of these 2 tracers: ^{11}C-LY2795050 has fast kinetics, whereas the kinetics of ^{11}C- GR103545 are protracted.

To our knowledge, ^{11}C-GR103545 has been the first KOR agonist radiotracer advanced to imaging applications in humans and ^{11}C-LY2795050 the first KOR antagonist tracer evaluated in humans—with both investigations taking place in our laboratory. As a result of these investigations, we now have a pair of agonist and antagonist radiotracers available for in vivo investigation of KOR.

The opioid receptors belong to the superfamily of G-protein–coupled receptors, and G-protein–coupled receptors are considered to have two states: a high affinity for agonists and a low-affinity state. Agonists bind only to the high-affinity state, whereas antagonists do not distinguish the low- and high-affinity states and bind to both. Hence, the availability of a pair of agonist (^{11}C-GR103545) and antagonist (^{11}C-LY2795050) KOR tracers for use in humans will provide unique opportunities to assess the potential changes not only in total receptor expression but also in receptor state under disease conditions, as seen in the studies of dopamine D_2/D_3 receptors with the agonist tracers ^{11}C-(+)-PHNO (^{11}C-(+)-4-propyl-9-hydroxynaphthoxazine),

TABLE 2
Binding Parameters Derived from MA1 Method

Region	V_T (mL/cm^3)		V_T/f_P (mL/cm^3)		BP_{ND}		BP_P (mL/cm^3)		BP_F (mL/cm^3)	
	Test	Retest	Test	Retest	Test	Retest	Test	Retest	Test	Retest
Amygdala	4.17 (13)	3.98 (13)	439 (18)	448 (26)	1.55 (19)	1.45 (21)	2.52 (15)	2.33 (17)	265 (21)	264 (30)
Insula	3.40 (11)	3.38 (10)	357 (15)	379 (22)	1.07 (17)	1.08 (14)	1.74 (11)	1.74 (8)	183 (15)	195 (20)
Ant. cingulate cortex	3.28 (12)	3.26 (11)	345 (16)	365 (23)	1.00 (14)	1.00 (15)	1.63 (12)	1.61 (11)	171 (17)	181 (22)
Globus pallidus	3.13 (11)	3.11 (13)	329 (16)	349 (26)	0.92 (23)	0.91 (21)	1.47 (16)	1.46 (20)	156 (21)	164 (30)
Putamen	2.90 (11)	2.91 (10)	305 (16)	326 (22)	0.77 (20)	0.79 (21)	1.25 (14)	1.27 (15)	132 (19)	142 (24)
Temporal cortex	2.65 (11)	2.64 (10)	278 (15)	295 (21)	0.62 (24)	0.62 (22)	0.99 (17)	0.99 (14)	104 (20)	111 (20)
Frontal cortex	2.64 (11)	2.63 (11)	278 (16)	294 (22)	0.61 (22)	0.61 (20)	0.98 (16)	0.98 (14)	104 (21)	110 (22)
Occipital cortex	2.47 (11)	2.45 (10)	259 (15)	274 (21)	0.51 (30)	0.51 (27)	0.81 (22)	0.81 (19)	85 (24)	90 (23)
Hippocampus	2.35 (11)	2.30 (11)	247 (15)	259 (25)	0.44 (30)	0.42 (34)	0.70 (25)	0.66 (30)	73 (26)	75 (38)
Caudate	2.28 (11)	2.28 (12)	240 (16)	256 (26)	0.40 (45)	0.40 (47)	0.62 (40)	0.63 (42)	66 (43)	72 (51)
Post. cingulate cortex	2.19 (12)	2.17 (13)	230 (17)	244 (24)	0.33 (43)	0.34 (47)	0.53 (36)	0.53 (43)	56 (38)	59 (46)
Thalamus	2.19 (9)	2.17 (9)	230 (15)	244 (23)	0.34 (43)	0.34 (47)	0.53 (37)	0.53 (43)	57 (39)	60 (45)
Centrum semiovale	2.19 (11)	2.14 (16)	230 (15)	241 (27)	0.34 (46)	0.31 (48)	0.54 (38)	0.50 (43)	56 (40)	56 (47)
Cerebellum	1.94 (16)	1.92 (16)	203 (19)	216 (26)	0.17 (0)	0.17 (0)	0.28 (16)	0.28 (16)	30 (19)	31 (26)

Ant. = anterior; Post. = posterior.

Data are mean of 16 subjects, with each value measured twice in test and retest scans. Data in parentheses are percentage coefficient of variation (intersubject variability).

TABLE 3
Test–Retest Reproducibility of Volume of Distribution

Region	2TC, V_T (mL/cm^3)			MA1, V_T (mL/cm^3)			MA1, V_T/f_P (mL/cm^3)		
	aTRV	TRV	ICC	aTRV	TRV	ICC	aTRV	TRV	ICC
Amygdala	9%	3% ± 11%	0.39 (-0.18;0.77)	12%	5% ± 14%	0.41 (-0.08;0.74)	18%	−1% ± 22%	0.55 (0.11;0.82)
Insula	7%	−1% ± 9%	0.58 (0.13;0.84)	7%	0% ± 9%	0.68 (0.31;0.87)	14%	−5% ± 18%	0.46 (-0.02;0.77)
Ant. cingulate cortex	8%	0% ± 10%	0.61 (0.19;0.84)	6%	0% ± 8%	0.78 (0.50;0.92)	14%	−5% ± 16%	0.60 (0.17;0.84)
Globus pallidus	8%	0% ± 10%	0.70 (0.32;0.89)	8%	1% ± 9%	0.74 (0.41;0.90)	15%	−4% ± 18%	0.55 (0.11;0.82)
Putamen	7%	−2% ± 8%	0.73 (0.37;0.90)	6%	0% ± 7%	0.81 (0.55;0.93)	13%	−6% ± 16%	0.57 (0.14;0.83)
Temporal cortex	9%	0% ± 11%	0.50 (0.04;0.79)	7%	0% ± 8%	0.70 (0.33;0.88)	13%	−5% ± 17%	0.50 (0.04;0.79)
Frontal cortex	8%	0% ± 10%	0.61 (0.20;0.84)	7%	0% ± 8%	0.74 (0.41;0.90)	13%	−5% ± 17%	0.54 (0.09;0.81)
Occipital cortex	9%	0% ± 11%	0.52 (0.06;0.80)	6%	1% ± 7%	0.77 (0.46;0.91)	13%	−5% ± 16%	0.52 (0.07;0.80)
Hippocampus	9%	2% ± 10%	0.63 (0.22;0.85)	8%	2% ± 9%	0.67 (0.28;0.87)	15%	−4% ± 18%	0.54 (0.10;0.81)
Caudate	7%	−2% ± 8%	0.77 (0.42;0.92)	6%	0% ± 7%	0.82 (0.56;0.93)	13%	−5% ± 16%	0.60 (0.18;0.84)
Post. cingulate cortex	9%	1% ± 11%	0.72 (0.37;0.89)	7%	1% ± 9%	0.76 (0.45;0.91)	14%	−5% ± 17%	0.61 (0.19;0.84)
Thalamus	8%	0% ± 9%	0.50 (0.04;0.79)	7%	1% ± 9%	0.54 (0.09;0.81)	15%	−5% ± 18%	0.51 (0.05;0.79)
Centrum semiovale	10%	4% ± 13%	0.57 (0.12;0.83)	10%	3% ± 13%	0.57 (0.14;0.83)	18%	−3% ± 20%	0.52 (0.06;0.80)
Cerebellum	7%	0% ± 9%	0.85 (0.63;0.94)	6%	1% ± 8%	0.89 (0.71;0.96)	13%	−5% ± 17%	0.64 (0.23;0.85)

Ant. = anterior; Post. = posterior.
2TC V_T estimates with relative SE > 10% or $k_4 < 0.001$ min^{-1} were excluded from calculation. Data within parentheses are 95% confidence intervals.

^{11}C-NPA ((−)-*N*-^{11}Cpropylnorapomorphine), or ^{11}C-MNPA ([*O*-methyl-^{11}C]2-methoxy-*N*-propylnorapomorphine) and the antagonist tracer ^{11}C-raclopride (*23*–*30*).

Given the excellent reproducibility of V_T estimates derived from PET imaging of KOR with ^{11}C-LY2795050 in the human brain and the involvement of KOR in several neuropsychiatric disorders, ^{11}C-LY2795050 is currently being used at our center in multiple clinical imaging studies to investigate the role of KOR in depression, posttraumatic stress disorder (*31*), cocaine addiction, and alcoholism.

CONCLUSION

In this study, we evaluated the reproducibility of binding parameters with ^{11}C-LY2795050 in humans and found that this novel KOR antagonist radiotracer provides excellent test–retest

TABLE 4
Test–Retest Reproducibility of Binding Potential

Region	BP_{ND}			BP_P (mL/cm^3)			BP_F (mL/cm^3)		
	aTRV	TRV	ICC	aTRV	TRV	ICC	aTRV	TRV	ICC
Amygdala	13%	7% ± 17%	0.56 (0.12;0.82)	16%	8% ± 20%	0.24 (−0.26;0.65)	22%	2% ± 27%	0.53 (0.07;0.80)
Insula	7%	−1% ± 8%	0.88 (0.71;0.96)	10%	0% ± 11%	0.36 (−0.14;0.71)	15%	−6% ± 19%	0.33 (−0.17;0.70)
Ant. cingulate cortex	5%	0% ± 7%	0.91 (0.76;0.97)	8%	1% ± 9%	0.67 (0.29;0.87)	14%	−5% ± 16%	0.61 (0.20;0.84)
Globus pallidus	9%	1% ± 11%	0.89 (0.71;0.96)	10%	1% ± 13%	0.76 (0.45;0.91)	18%	−4% ± 20%	0.62 (0.20;0.85)
Putamen	7%	−2% ± 8%	0.93 (0.82;0.98)	7%	−2% ± 8%	0.85 (0.62;0.94)	14%	−7% ± 15%	0.66 (0.27;0.87)
Temporal cortex	6%	−1% ± 8%	0.95 (0.87;0.98)	9%	−1% ± 10%	0.77 (0.47;0.91)	15%	−6% ± 18%	0.59 (0.16;0.83)
Frontal cortex	5%	−1% ± 7%	0.94 (0.83;0.98)	8%	0% ± 10%	0.76 (0.45;0.91)	15%	−6% ± 18%	0.63 (0.22;0.85)
Occipital cortex	9%	−1% ± 13%	0.95 (0.87;0.98)	10%	0% ± 12%	0.86 (0.66;0.95)	14%	−6% ± 18%	0.71 (0.36;0.89)
Hippocampus	15%	7% ± 17%	0.89 (0.72;0.96)	17%	7% ± 18%	0.79 (0.51;0.92)	22%	2% ± 25%	0.70 (0.33;0.88)
Caudate	10%	−2% ± 16%	0.98 (0.95;0.99)	10%	−1% ± 14%	0.96 (0.90;0.99)	15%	−7% ± 17%	0.88 (0.69;0.95)
Post. cingulate cortex	22%	9% ± 44%	0.92 (0.80;0.97)	24%	10% ± 44%	0.86 (0.66;0.95)	27%	5% ± 45%	0.82 (0.57;0.93)
Thalamus	31%	22% ± 81%	0.96 (0.90;0.99)	36%	24% ± 86%	0.91 (0.77;0.97)	45%	22% ± 98%	0.83 (0.59;0.94)
Centrum semiovale	33%	16% ± 59%	0.82 (0.58;0.93)	35%	15% ± 60%	0.70 (0.34;0.88)	42%	11% ± 64%	0.67 (0.29;0.87)

Ant. = anterior; Post. = posterior.
Data within parentheses are 95% confidence intervals.

reproducibility, with absolute TRV of no more than 10% in any brain region except the amygdala. The results from the present study strongly support the use of ^{11}C-LY2795050 as a PET radiotracer to image and quantitate KOR in humans with high reliability.

DISCLOSURE

The costs of publication of this article were defrayed in part by the payment of page charges. Therefore, and solely to indicate this fact, this article is hereby marked "advertisement" in accordance with 18 USC section 1734. This study was supported by Eli Lilly and Co. and by a research grant from NIMH (1 R01 MH091537). This publication was also made possible by CTSA grant UL1 RR024139 from the National Center for Research Resources (NCRR) and the National Center for Advancing Translational Sciences (NCATS), components of the National Institutes of Health (NIH). No potential conflict of interest relevant to this article was reported. The contents of this article are solely the responsibility of the authors and do not necessarily represent the official view of NIH.

ACKNOWLEDGMENT

We appreciate the excellent technical assistance of the staff at the Yale University PET Center.

REFERENCES

1. Van't Veer A, Carlezon WA Jr. Role of kappa-opioid receptors in stress and anxiety-related behavior. *Psychopharmacology (Berl).* 2013;229:435–452.
2. Mello NK, Negus SS. Interactions between kappa opioid agonists and cocaine: preclinical studies. *Ann N Y Acad Sci.* 2000;909:104–132.
3. Tenore PL. Psychotherapeutic benefits of opioid agonist therapy. *J Addict Dis.* 2008;27:49–65.
4. Gerra G, Fantoma A, Zaimovic A. Naltrexone and buprenorphine combination in the treatment of opioid dependence. *J Psychopharmacol.* 2006;20:806–814.
5. de Lanerolle NC, Williamson A, Meredith C, et al. Dynorphin and the kappa 1 ligand [^{3}H]U69,593 binding in the human epileptogenic hippocampus. *Epilepsy Res.* 1997;28:189–205.
6. Mathieu-Kia AM, Fan LQ, Kreek MJ, Simon EJ, Hiller JM. Mu-, delta- and kappa-opioid receptor populations are differentially altered in distinct areas of postmortem brains of Alzheimer's disease patients. *Brain Res.* 2001;893:121–134.
7. Carr GV, Bangasser DA, Bethea T, Young M, Valentino RJ, Lucki I. Antidepressant-like effects of kappa-opioid receptor antagonists in Wistar Kyoto rats. *Neuropsychopharmacology.* 2010;35:752–763.
8. Schank JR, Goldstein AL, Rowe KE, et al. The kappa opioid receptor antagonist JDTic attenuates alcohol seeking and withdrawal anxiety. *Addict Biol.* 2012;17:634–647.
9. Zheng MQ, Nabulsi N, Kim SJ, et al. Synthesis and evaluation of ^{11}C-LY2795050 as a kappa-opioid receptor antagonist radiotracer for PET imaging. *J Nucl Med.* 2013;54:455–463.
10. Huang Y, Zheng MQ, Gerdes JM. Development of effective PET and SPECT imaging agents for the serotonin transporter: has a twenty-year journey reached its destination? *Curr Top Med Chem.* 2010;10:1499–1526.
11. Kim SJ, Zheng MQ, Nabulsi N, et al. Determination of the in vivo selectivity of a new kappa-opioid receptor antagonist PET tracer C-11-LY2795050 in the rhesus monkey. *J Nucl Med.* 2013;54:1668–1674.
12. Naganawa M, Zheng MQ, Nabulsi N, et al. Kinetic modeling of ^{11}C-LY2795050, a novel antagonist radiotracer for PET imaging of the kappa opioid receptor in humans. *J Cereb Blood Flow Metab.* 2014;34:1818–1825.
13. Carson RE, Barker WC, Liow JS, Johnson CA. Design of a motion-compensation OSEM list-mode algorithm for resolution-recovery reconstruction for the HRRT. *IEEE 2003 Nuclear Science Symposium Conference Record.* 2003;5:3281–3285.
14. Jin X, Mulnix T, Gallezot JD, Carson RE. Evaluation of motion correction methods in human brain PET imaging: a simulation study based on human motion data. *Med Phys.* 2013;40:102503.
15. Tzourio-Mazoyer N, Landeau B, Papathanassiou D, et al. Automated anatomical labeling of activations in SPM using a macroscopic anatomical parcellation of the MNI MRI single-subject brain. *Neuroimage.* 2002;15:273–289.
16. Holmes CJ, Hoge R, Collins L, Woods R, Toga AW, Evans AC. Enhancement of MR images using registration for signal averaging. *J Comput Assist Tomogr.* 1998;22:324–333.
17. Ichise M, Liow JS, Lu JQ, et al. Linearized reference tissue parametric imaging methods: application to [^{11}C]DASB positron emission tomography studies of the serotonin transporter in human brain. *J Cereb Blood Flow Metab.* 2003;23:1096–1112.
18. Innis RB, Cunningham VJ, Delforge J, et al. Consensus nomenclature for in vivo imaging of reversibly binding radioligands. *J Cereb Blood Flow Metab.* 2007;27:1533–1539.
19. Henriksen G, Willoch F. Imaging of opioid receptors in the central nervous system. *Brain.* 2008;131:1171–1196.
20. Talbot PS, Narendran R, Butelman ER, et al. ^{11}C-GR103545, a radiotracer for imaging kappa-opioid receptors in vivo with PET: synthesis and evaluation in baboons. *J Nucl Med.* 2005;46:484–494.
21. Tomasi G, Nabulsi N, Zheng MQ, et al. Determination of in vivo Bmax and Kd for ^{11}C-GR103545, an agonist PET tracer for kappa-opioid receptors: a study in nonhuman primates. *J Nucl Med.* 2013;54:600–608.
22. Naganawa M, Jacobsen LK, Zheng MQ, et al. Evaluation of the agonist PET radioligand [^{11}C]GR103545 to image kappa opioid receptor in humans: kinetic model selection, test-retest reproducibility and receptor occupancy by the antagonist PF-04455242. *Neuroimage.* 2014;99:69–79.
23. Boileau I, Payer D, Chugani B, et al. The D2/3 dopamine receptor in pathological gambling: a positron emission tomography study with [^{11}C]-(+)-propyl-hexahydro-naphtho-oxazin and [^{11}C]raclopride. *Addiction.* 2013;108:953–963.
24. Caravaggio F, Raitsin S, Gerretsen P, Nakajima S, Wilson A, Graff-Guerrero A. Ventral striatum binding of a dopamine $D_{2/3}$ receptor agonist but not antagonist predicts normal body mass index. *Biol Psychiatry.* March 27, 2013 [Epub ahead of print].
25. Graff-Guerrero A, Willeit M, Ginovart N, et al. Brain region binding of the D2/3 agonist [^{11}C]-(+)-PHNO and the D2/3 antagonist [^{11}C]raclopride in healthy humans. *Hum Brain Mapp.* 2008;29:400–410.
26. Gallezot JD, Kloczynski T, Weinzimmer D, et al. Imaging nicotine- and amphetamine-induced dopamine release in rhesus monkeys with [^{11}C]PHNO vs [^{11}C]raclopride PET. *Neuropsychopharmacology.* 2014;39:866–874.
27. Narendran R, Mason NS, Laymon CM, et al. A comparative evaluation of the dopamine $D_{2/3}$ agonist radiotracer [^{11}C](-)-N-propyl-norapomorphine and antagonist [^{11}C]raclopride to measure amphetamine-induced dopamine release in the human striatum. *J Pharmacol Exp Ther.* 2010;333:533–539.
28. Seneca N, Finnema SJ, Farde L, et al. Effect of amphetamine on dopamine D2 receptor binding in nonhuman primate brain: a comparison of the agonist radioligand [^{11}C]MNPA and antagonist [^{11}C]raclopride. *Synapse.* 2006;59:260–269.
29. Tsukada H, Ohba H, Nishiyama S, Kakiuchi T. Differential effects of stress on [^{11}C]raclopride and [^{11}C]MNPA binding to striatal D2/D3 dopamine receptors: a PET study in conscious monkeys. *Synapse.* 2011;65:84–89.
30. Kodaka F, Ito H, Kimura Y, et al. Test-retest reproducibility of dopamine D2/3 receptor binding in human brain measured by PET with [^{11}C]MNPA and [^{11}C] raclopride. *Eur J Nucl Med Mol Imaging.* 2013;40:574–579.
31. Pietrzak RH, Naganawa M, Huang Y, et al. Association of in vivo kappa-opioid receptor availability and the transdiagnostic dimensional expression of trauma-related psychopathology. *JAMA Psychiatry.* 2014;71:1262–1270.